Validating a Model for Bluff-Body Burners Using the HM1 Turbulent Nonpremixed Flame

Osama A. Marzouk*

University of Buraimi, College of Engineering, P.O. Box 890, P.C. 512, Al Buraimi, Sultanate of Oman

Abstract: We conducted computational fluid dynamics modeling of the bluff-body stabilized flame known as HM1, which was studied experimentally in detail at the University of Sydney to provide modelers with sufficient measurements to allow validation of their computational models. This benchmark flame is turbulent nonpremixed with a fuel-jet composed of 50% hydrogen and 50% methane by volume (hence the acronym HM) surrounded by a coflow of air, which is bounded by the walls of a wind tunnel. We successfully perfromed computational modeling of this flame, utilizing the published data about the problem settings and using a customized solver based on the open-source control-volume toolkit OpenFOAM. We describe the model settings and report the results of our predictions and show how they agree well with the measurements in terms of axial and radial profiles of miscellaneous flow variables. We conducted the simulation employing two meshes and obtained a reasonably mesh-idepenedent solution. The results suggest that the model can provide satisfactory results with as few as 10000 wedge-type computational cells. The model thus represents a free and fast computer tool to assist in the design of industrial bluff-body burners that possess similarity with the analyzed burner here.

Keywords: Flame, nonpremixed, TNF, CFD, OpenFOAM, bluff-body, combustion.

1. INTRODUCTION

A flame is a self-sustaining combustion zone that is produced when a burnable substance undergoes combustion. Flames are localized, thus occupy a small portion of the burnable substance at any one time; rather than occurring uniformly throughout it.

There are two main categories of flames [1] based on the nature of mixing between the oxidizer and the burnable substance (fuel). The first category is the premixed flame, where the fuel and the oxidizer are mixed before they are introduced into the combustion zone. These flames are characterized by being non-luminous with colors varying typically from yellow to green. The flame is not luminous due to the absence of soot (emission particulates), because formed soot particles in a premixed flame meet the oxidizer within the flame and react with it; consequently premixed flame are generally expected to have small amounts of soot particles. The core of the Bunsen burner flame is an example of such flames. The second main category of flames is called nonpremixed or diffusion flames. They are called nonpremixed flames because the fuel and oxidizer are introduced as separate streams into the combustion zone. They are called diffusion flames because the chemical reactions can take place only where fuel and oxidizer are mixed on the molecular level through molecular diffusion. The time scale of reaction is much shorter than the time scale for diffusion; thus diffusion is the rate-limiting phenomenon because the oxidizer and fuel diffuse into each other very slowly. Therefore, nonpremixed flames tend to burn slower than premixed flames. Nonpremixed flames are typically characterized by the emission of soot particles because of insufficient oxidizer within the flame, leading to a typical lumnous orange color. Nonpremixed flames are much more encountered in daily life than premixed flames; examples include candle flame, matchstick flame, and the outer cone of the Bunsen burner flame.

Another classification of flames is based on the nature of the gases, which can be laminar or turbulent. Whereas the core of the Bunsen burner flame is an example of a laminar premixed flame and the candle flame and the outer cone of the Bunsen burner are examples of a laminar nonpremixed flame; turbulent flames are found in practical fields often and play an important role in industrial processes and power generation. Commercial combustion demands high supply velocities of the reactants, well beyond the threshold of a laminar flame. On the other hand, laminar flames exhibit relatively simple phenomena and thus are favored in academic studies to understand and build mathematical models for flame combustion which can be later extended to turbulent flames [2, 3]. Moreover, turbulent nonpremixed flames (TNF) are favored to the premixed counterparts in a large number of industrial systems for two reasons: First, nonpremixed burners are simpler to design and to build because they do not require a perfect reactant mixing with set proportions. Second, nonpremixed flames are safer to operate as they do not exhibit propagation

*Address correspondence to this author at the University of Buraimi, College of Engineering, P.O. Box 890, P.C. 512, Al Buraimi, Sultanate of Oman:
Tel: +968-91173908; Fax: +968-25651265;
E-mail: osama.m@uob.edu.om; omarzouk@vt.edu

E-ISSN: 2409-5826/16

speeds and cannot flashback or autoginite in undesirable locations. With turbulence introduced, the term diffusion that strictly applies to molecular diffusion of chemical species is still a controlling mechanism for turbulent nonpremixed flames; initially turbulent convection mixes the fuel and oxidizer macroscopically, and eventually molecular diffusion completes the process so that chemical reaction can take place.

Turbulent nonpremixed flames with high jet velocities are commercially attractive but they tend to be unstable, exhibiting undesirable phenomena such as blow-off and lift-off. High velocity burners in aluminum, steel, and glass industries enjoy another advantage, being inherently low NOx (nitrogen oxides) producers because they entrain significant amounts of cool furnace gases into the flame envelope before the complete combustion [4]. Lowering the in-flame temperature retards the thermal NOx whose formation requires high temperatures [5]. Other combustion settings exhibiting reduced emissions include lean fuel concentration and low temperatures. However, these settings are harsh and again the flame tends to be unstable [6]. Stabilizing such flames (anchoring the flames) in industrial burners can be achieved through three techniques [7]. One technique uses a pilot burner [8] (also called pilot light), in which a small auxiliary pilot flame burns initially to ignite the main burner [9]. This pilot flame can then be deactivated if the flame is not known to have any instability problem [10], but is kept in continuous operation when it should serve to maintain a stable burner operation without flame extinction [11]. The pilot flame can be implemented as a premixed flame or as an electric igniter. Pilot-stabilized flames are very stable for a wide range of operation conditions [12]; however, they incur the complication of extra pilot burner [13] and also the energy penalty (whether chemical source or electric source) [14] to allow such an active stabilization technique. Another stabilization technique uses swirl (recirculation). A recirculation zone provides proper conditions where reactions can take place. However, swirl can lead to some unfavorable effects; a precessing vortex core can cause combustion instability. In addition, swirl affects the unsteady anchoring location of the flame, which can cause further combustion instability, as found experimentally for a gas turbine combustor [15]. The third stabilization technique for turbulent nonpremixed flames is the one we consider here, which is the use of a bluff-body burner (also called flame holder). When a bluff body is placed in a high velocity stream of reactants, the flow is slowed down in the wake, which enables reactions to proceed to ignition. Bluff-body burners are of special importance because they share similar features with those burners used in many industrial applications and it is therefore very useful to have reliable modeling tools to analyze and predict the flow fields and operation for these flames [16]. This type of TNF burner serves as a good benchmark problem for computational combustion modeling as they form a reasonable compromise, exhibiting some of the complications associated with practical combustors while preserving relatively simple and well-defined boundary conditions.

The particular bluff-body stabilized flame we model here is the one studied experimentally at the University of Sydney [17] and is the only bluff-body flame configuration referenced online by the International Workshop on Measurement and Computation of Turbulent Nonpremixed Flames (TNF Workshop) [18]. This flame is referred to as HM1, due to the composition of the gaseous fuel stream being a mixture of hydrogen and methane (with equal mole/volume fractions of 50% each). This flame is an attractive benchmark problem not just because of the practicality of its high velocity bluff-body burner, but also because of the detailed information about the problem settings and the measurements which enable us to establish a proper model for it without major deviations from the geometric or input conditions, which consequently should lead in principle to consistent and meaningful comparisons between the model predictions and the measurements.

The HM1 benchmark flame has been utilized in earlier computational studies, such as the one carried out by Yan *et al*. [19]. In their work, the axisymmetric governing equations were solved using a general purpose CFD code employing a structured multi-block grid based on general nonorthogonal coordinates and finite-volume methods. The nonuniform grid consisted of 3 blocks having about 18000 cells concentrated near the bluff body. They used the flamelet model [20] for the turbulence-chemistry interaction. Their main aim was to investigate the effect of the turbulence modeling on the overall prediction and they tried three different turbulence models (basic k-epsilon model, modified k-epsilon model with varied anisotropy parameter, and the explicit algebraic stress model). We note that the coefficient $C_{\epsilon 2}$ in their basic model was 1.83, whereas the standard value is 1.92 [21]. They concluded that the overall predictions depend on the turbulence model selection. The predictions were fairly reasonable but there were notable errors in the radial profile predictions for the r.m.s. of the axial velocity fluctuations, r.m.s. of the mixture fraction variance, and mean mass fraction of CO_2 for all of the 3 turbulence models.

Liu *et al*. [22] also treated the problem as axisymmetric and employed a structured grid with a total of 6912 cells (72 cells in the axial direction and 96 cells in the radial direction). The turbulence-chemistry interaction was modeled using the joint probability density function (PDF) [23]. The authors analyzed the sensitivity of the predictions to the mixing model for the PDF calculations which represents the effects of molecular diffusion. Two different mixing models were attempted, namely the interaction by exchange with the mean (IEM) model and the Euclidean minimum spanning tree (EMST). Some predictions of the radial profiles of the mean mixture fraction and its r.m.s. showed strong deviations near the centerline, where the model predicted much smaller values than the measurements.

Odedra and Malalasekera [24] again treated the problem as axisymmetric in their modeling, and performed the Favre-averaged Navier Stokes simulation using steady and unsteady flamelet models. They handled the unsteadiness through a post-processing fashion utilizing the Eulerian particle flamelet model (EPFM). Their modeling framework was the commercial CFD software FLUENT 6.1 (currently ANSYS FLUENT [25]), in which they chose the Reynolds stress model (RSM) to represent the turbulence effects. The main domain (excluding upstream extension) was discretized into 44200 quadrilateral cells (260 × 170). The predicted radial profiles of the axial velocity were in good agreement with the measurements, but the radial velocity profiles showed large errors. The mass fraction of H_2 was overpredicted near the centerline, but rapidly merged well with the measurement as the radial coordinate increases.

We point out that other computational studies (Raman and Pitsch [26], Kempf *et al*. [27], and James *et al*. [28]) addressed this benchmark flame but using the costly large eddy simulation (LES) and 3-dimensional geometry. Given the humongous computational resources and time demanded by this modeling strategy, these studies are skipped here as we focus on practical approaches for mainstream engineering and industry applications [29].

Our simulations are based on the open-source framework OpenFOAM (Open Field Operation And Manipulation) [30]. The base solver is readily available for any user and our validations (through comparing profiles of flow field variables at various spatial locations in the flame) give interested researchers a motivation to rely more on this framework for similar combustion problems. In fact, this framework allows the modeling of much more complicated problems, including coal combustion and gaseous thermal radiation.

2. CONFIGURATION OF THE HM1 FLAME

Figure **1** shows a sketch for the burner along with the boundaries of the wind tunnel having a square cross-section. The burner resembles a very thick vertical tube, where the fuel-jet flows up out of the central orifice. The burner is immersed in a coflow stream of air passing through the wind tunnel. The thick face of the bluff body leads to the formation of a recirculation zone that produces sufficiently hot gases there to stabilize the flame and keep it anchored to the burner.

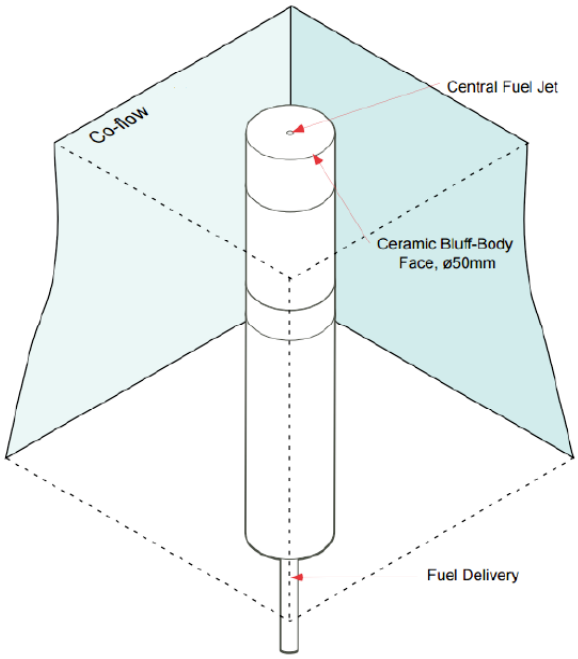

Figure 1: Sketch of the bluff-body burner of the HM1 flame (adapted from [17]).

The following data in Table **1** correspond to the flame code (B4F3) [31], which is the reference flame in our work.

If the fuel-jet velocity increases, then at a certain threshold (blow-off velocity) the flame can be extinguished downstream of the recirculation zone and may even reignite further downstream. From the data in Table **1**, one sees that the HM1 flame is approximately at 50% of the blow-off limit and thus these phenomena are not encountered.

Table 1: Experimental Parameters of the HM1 Flame (B4F3)

Wind tunnel dimensions (mm)	305 × 305
Fuel-jet radius (mm)	1.8
Bluff-body radius (mm)	25
Fuel-jet mixture	CH_4/H_2 (50/50 % by volume)
Fuel-jet velocity	118 m/s
Blow-off velocity (m/s)	235
Coflow air velocity (m/s)	40
Coflow turbulence intensity	2%
Mass fraction of O_2 in coflow	0.233 (21% by volume)
Mass fraction of N_2 in coflow	0.767 (79% by volume)

An image of the HM1 flame is shown in Figure **2**. It is noteworthy that the flame has a blue color instead of a luminous orange as common for a nonpremixed flame due to the soot formation. The explanation for this feature also explains the addition of H_2 to the fuel instead of burning pure CH_4. The added H_2 reduces the soot formation [32] as it leads to a recirculation zone which is nearly clean from soot. Pure CH_4 flames generally feature the formation of soot in the recirculation zone. When this soot is convected downstream, it causes undesirable interference with the Raman signal, and thus degrades the accuracy of the measurements of the mass fractions of species. Adding H_2 (as done here) to CH_4 successfully makes the recirculation zone free from soot.

The axial and radial velocities were measured simultaneously using the laser Doppler velocimetry (LDV) method. A two-color argon-ion laser beam with 5W was used. Instantaneous values (at a single point) of temperature and mass fraction of species were collected using Raman, Rayleigh, and laser-induced fluorescence (LIF) measurements.

3. COMPUTATIONAL MODELING

The simulation used a modified version of the *reactingFoam* [33] solver, distributed as part of the OpenFOAM open-source finite-volume multi-solver toolkit that is based on C++ computer codes and miscellaneous text files to describe the problem geometry as well as the initial conditions, boundary conditions, physical modeling parameters, reaction mechanism steps, and numerical solver settings. The modification was to add the differential diffusion in the enthalpy-based energy equation (last term of Equation 4) due to the difference in the effective species and thermal diffusivities. This corresponds to the assumption that Lewis number is unity for all species (*i.e.*, equal molecular mass and molecular thermal diffusivities for each species) and also the turbulent Lewis number is unity (*i.e.*, equal turbulent mass and turbulent thermal diffusivities). In fact, this differential diffusion is usually neglected while modeling turbulent reacting flows [34]. All the flow variables are stored at

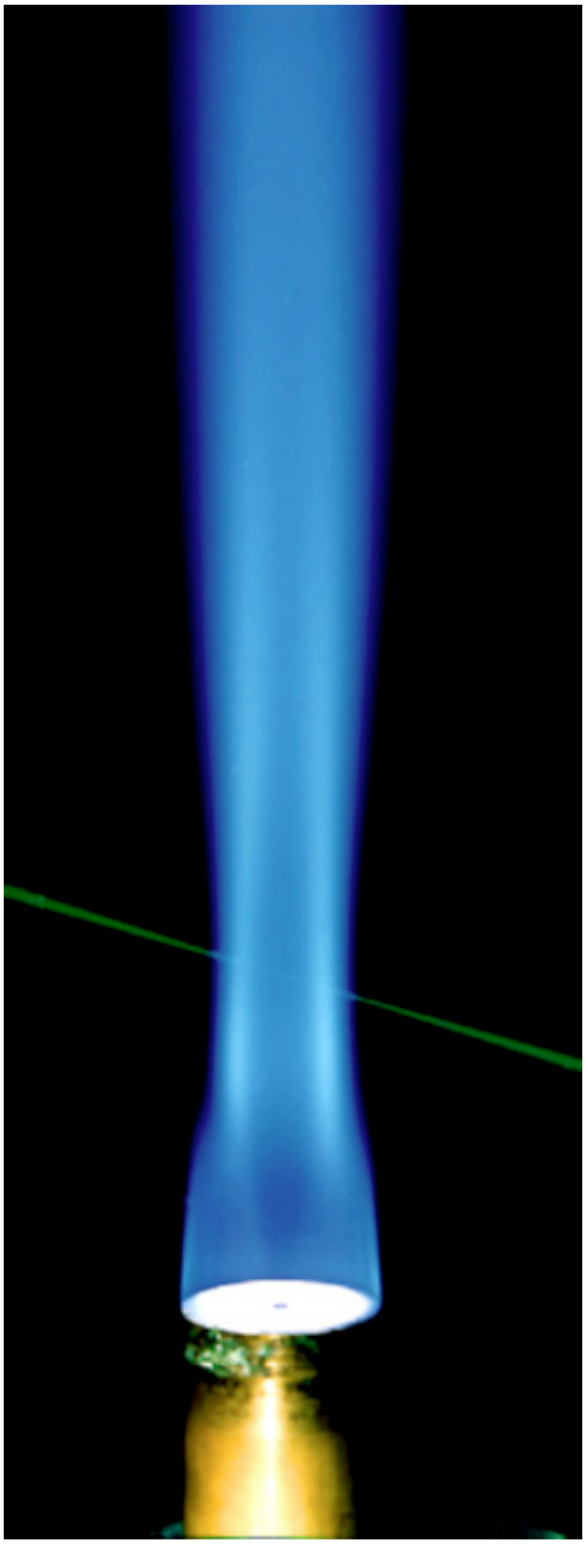

Figure 2: Photo of the HM1 flame [17].

the cell centers (not face centers) although interpolations are heavily used during the simulation to obtain needed face values of variables but as temporary quantities. Thus, the mesh arrangement is collocated (not staggered).

The proper conservation equations of mass, momentum, energy (in terms of the specific enthalpy), and species mass fractions in OpenFOAM, respectively, are:

$$\frac{\partial \rho}{\partial t} + \nabla .\left(\rho \vec{U} \right) = 0 \tag{1}$$

$$\begin{aligned} &\frac{\partial \rho}{\partial t} + \nabla .\left(\rho \overrightarrow{\overrightarrow{UU}} \right) - \nabla .\left(\mu_{eff} \overrightarrow{\overrightarrow{\nabla U}} \right) = \\ &-\overrightarrow{\nabla p} + \nabla .\left(\mu_{eff} \left[\overrightarrow{\overrightarrow{\nabla U}}^{T} - \vec{\vec{I}} \frac{2}{3} tr\left(\overrightarrow{\overrightarrow{\nabla U}} \right) \right] - \vec{\vec{I}} \frac{2}{3} \rho k \right) + \rho \vec{g} \end{aligned} \tag{2}$$

$$\frac{\partial \left(\rho Y_i \right)}{\partial t} + \nabla .\left(\rho \vec{U} Y_i \right) - \nabla .\left(\rho D_{i,eff} \overrightarrow{\nabla Y_i} \right) = k \mathbb{R}_i \tag{3}$$

$$\begin{aligned} &\frac{\partial \left(\rho h \right)}{\partial t} + \nabla .\left(\rho \vec{U} h \right) - \nabla .\left(\alpha_{eff} \overrightarrow{\nabla h} \right) = \\ &\frac{Dp}{Dt} + \sum_{i=1}^{Ns} \left(\nabla .\left\langle h_i \left[\rho D_{i,eff} - \alpha_{eff} \right] \right\rangle \overrightarrow{\nabla Y_i} \right) \end{aligned} \tag{4}$$

In the above formulas, a single arrow indicates a vector field whereas two arrows indicate a tensor field. The density is ρ, the velocity vector is $\vec{U}$, the effective dynamic viscosity is μ_{eff}, the pressure is *p*, the turbulent kinetic energy (per unit mass) is k, the effective kinematic mass diffusivity of the i[th] species is $D_{i,eff}$, the mass fraction of the i[th] species is Y_i, the reactive volume fraction (nonzero positive dimensionless scaling multiplier with an upper limit of unity) is κ, the unscaled chemical reaction source of the i[th] species is $\mathbb{R}_i$, the mixture's specific static enthalpy is h, the specific static enthalpy of the i[th] species is h_i, the effective dynamic thermal diffusivity is α_{eff}, and the total number of species is N_s. The trace operator is (tr), the identity tensor is $\vec{\vec{I}}$, the substantial time derivative is $\frac{D}{Dt}$, and the transpose operator is a superscript (T). Turbulence-chemistry interaction is based on the Chalmers' partially stirred reactor (CPaSR) model [35]. We express the momentum equation (Equation 2) above in a form that emphasizes which terms are treated implicitly (which are the LHS terms) and which term are treated explicitly (which are the RHS terms). A tailored k-epsilon model is used for the turbulence modeling, where a value of 1.6 is used instead of the standard value of 1.44 for the model constant $C_{\in 1}$, because the adjusted value suits better self-similar round jets [24, 36]. This modification was also found to give desirable numerical stability [37]. With the simplifying assumption that laminar and turbulent Schmidt numbers for all species are unity, $\rho D_{i,eff}$ is replaced by μ_{eff} in Equations 3 and 4, which now take the following forms:

$$\frac{\partial \left(\rho Y_i \right)}{\partial t} + \nabla .\left(\rho \vec{U} Y_i \right) - \nabla .\left(\mu_{eff} \overrightarrow{\nabla Y_i} \right) = k \mathbb{R}_i \tag{5}$$

$$\begin{aligned} &\frac{\partial \left(\rho h_i \right)}{\partial t} + \nabla .\left(\rho \vec{U} h \right) - \nabla .\left(\alpha_{eff} \overrightarrow{\nabla h} \right) = \\ &\frac{Dp}{Dt} + \sum_{i=1}^{N_s} \left(\nabla .\left\langle h_i \left[\mu_{eff} - \alpha_{eff} \right] \right\rangle \overrightarrow{\nabla Y_i} \right) \end{aligned} \tag{6}$$

The PISO (Pressure Implicit Splitting of Operators) pressure/velocity coupling scheme is used. In this scheme, the primitive form of the conservation of mass (Equation 1) is not solved. Instead, mathematical manipulation leads to an elliptic Poisson-type equation for the pressure, whose source term is dependent on the velocity field, and an explicit equation for the velocity relating it to the pressure gradient. To better explain the scheme, we consider an incompressible fluid and write a semi-discretized version of the momentum equation (Equation 2) as [38]:

$$a_p \overrightarrow{U_p} = H\left(\vec{U} \right) - \overrightarrow{\nabla p} \tag{7}$$

where a_p is a constant coefficient for each cell that depends on the geometry and discretization scheme used for the momentum equation; it is the coefficient multiplying the cell's own velocity $\overrightarrow{U_p}$. The vector source function $H(\vec{U})$ accounts for the discretized terms of the momentum equation excluding the pressure gradient term (thus, accounts for the transport part only). The elliptic pressure equation and the explicit velocity correction equation, respectively, can be derived directly from Equation 7 as:

$$\nabla .\left(\frac{1}{a_p} \overrightarrow{\nabla p} \right) = \nabla .\left(\frac{1}{a_p} H\left(\overrightarrow{U^*} \right) \right) \tag{8}$$

$$\overrightarrow{U_P^{corr}} = \frac{1}{a_p} \mathrm{H}\left(\overrightarrow{U^*} \right) - \frac{1}{a_p} \overrightarrow{\nabla p} \tag{9}$$

Equation 9 is essentially Equation 7 after dividing both sides by a_p. For better clarification, a superscript asterisk is used to emphasize that this velocity $\overrightarrow{U^*}$ is temporary and requires later correction to give the corrected velocity $\overrightarrow{U_P^{corr}}$ in the left-hand side of Equation 9. Equation 8 can be derived from Equation 9 by taking the divergence of both sides, and enforcing a divergence-free corrected velocity field, which is the reduced form of the conservation of mass for an incompressible fluid as can be seen from Equation 1, viz.

$$\nabla . \overrightarrow{U^{corr}} = 0 \quad (10)$$

The momentum equation (Equation 2) is first solved using the current pressure field and a temporary velocity field is obtained that does not perfectly satisfy the conservation of mass. This is followed by a three-step PISO sequence:

1 First, the pressure equation (depicted by Equation 8) is solved.

2 Then, the obtained pressure field is used to update the mass fluxes at the cell faces.

3 Finally, the temporary velocity field is corrected (using the explicit correction formula as depicted by Equation 9) to take into account the new resolved pressure field.

This sequence represents a single PISO correction, which can be repeated for better performance. The governing equations are corrected about five times in every time step in a sequential manner. In each of these corrections, about two PISO corrections are done. Thus, the momentum equation, species mass-fraction equations, and energy equation are solved five times per time step, whereas the pressure equation is solved ten times in every time step (and also the mass fluxes and temporary velocity field are corrected). In the solver, the following order is followed:

1 The momentum equation (Equation 2) is solved,

2 Then, the unity-Schmidt numbers species equations (Equations 5) are solved,

3 Then, the unity-Schmidt numbers energy equation (Equation 6) is solved,

4 Finally, the PISO correction loop is carried out.

The algebraic systems resulting from applying the finite volume discretization at the cell level are solved using iterative solvers for each equation.

OpenFOAM always adopt 3-dimensional meshes even when modeling 2-dimensional problems, as we have here. In the present axisymmetric configuration, a wedge-type domain is constructed as shown in Figure **3**, with a full-wedge-angle of 5°. To allow the incoming fuel stream and oxidizer stream to build a profile at the domain inlet, the domain is extended in the upstream direction by 4 jet radii for the fuel-jet and one bluff-body radius for the oxidizer coflow. The figure shows 5 blocks representing the structured non-uniform multi-block mesh. Cells near the centerline and

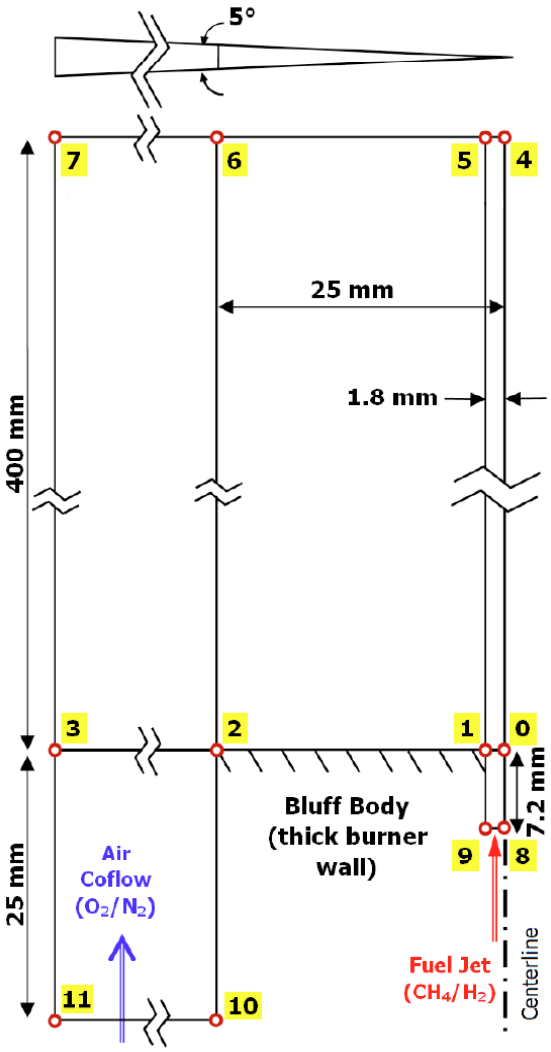

Figure 3: Computational domain and reactants streams.

near the burner have the smallest volume. The blocks are identified by 12 grid points (numbered from 0 to 11) as shown in the figure. This numbering is interpreted by an OpenFOAM built-in utility to build the wedge geometry properly. The axisymmetric model cannot handle the square cross-section coflow boundary. To circumvent this, the coflow passage is approximated by an annulus (cross section-area equivalence leads to an outer radius of 172mm). The impact of this geometric change is trivial because the flow variables variations decay well before such a large radial distance. We solved the problem with two meshes: level-1 mesh with 12836 cells and level-2 mesh with 37202 cells. In level-1 mesh, the axial cell size at the burner face is 1.89mm, and increases to 9.44mm at the outflow boundary. For level-2 mesh, these values drop to 0.4mm (21%) and 8.20mm (87%), respectively. In level-1 mesh, the radial cell size at the centerline is 0.223mm and it drops to 0.126mm (57%) for level -2 mesh.

At the downstream exit boundary, a pressure boundary condition is used, whereas a zero-gradient pressure condition is imposed at the inlet. The wall-function treatment is employed at the walls. The fuel jet and air coflow compositions are specified in terms of the species mass fractions according to the available experimental data. The temperature and species mass fractions are fixed at the inlet boundaries, whereas a zero-gradient condition is specified at the outlet boundaries. The fuel-jet temperature is set to 298K, and the coflow temperature is set to 300K. At the front and back faces of the wedge, a special boundary condition called wedge is applied in OpenFOAM, such that the solver handles the axisymmetry properly.

4. RESULTS

We present the modeling results in the form of radial and axial profiles of the axial and radial velocity components, the CH_4 (as a reactant) and H_2O (as a product) mass fractions, and the temperature. Before comparing the model predictions (for two meshes) with measurements, we point out that the reported measurements for the scalar variables (temperature and mass fractions) are available in both ensemble

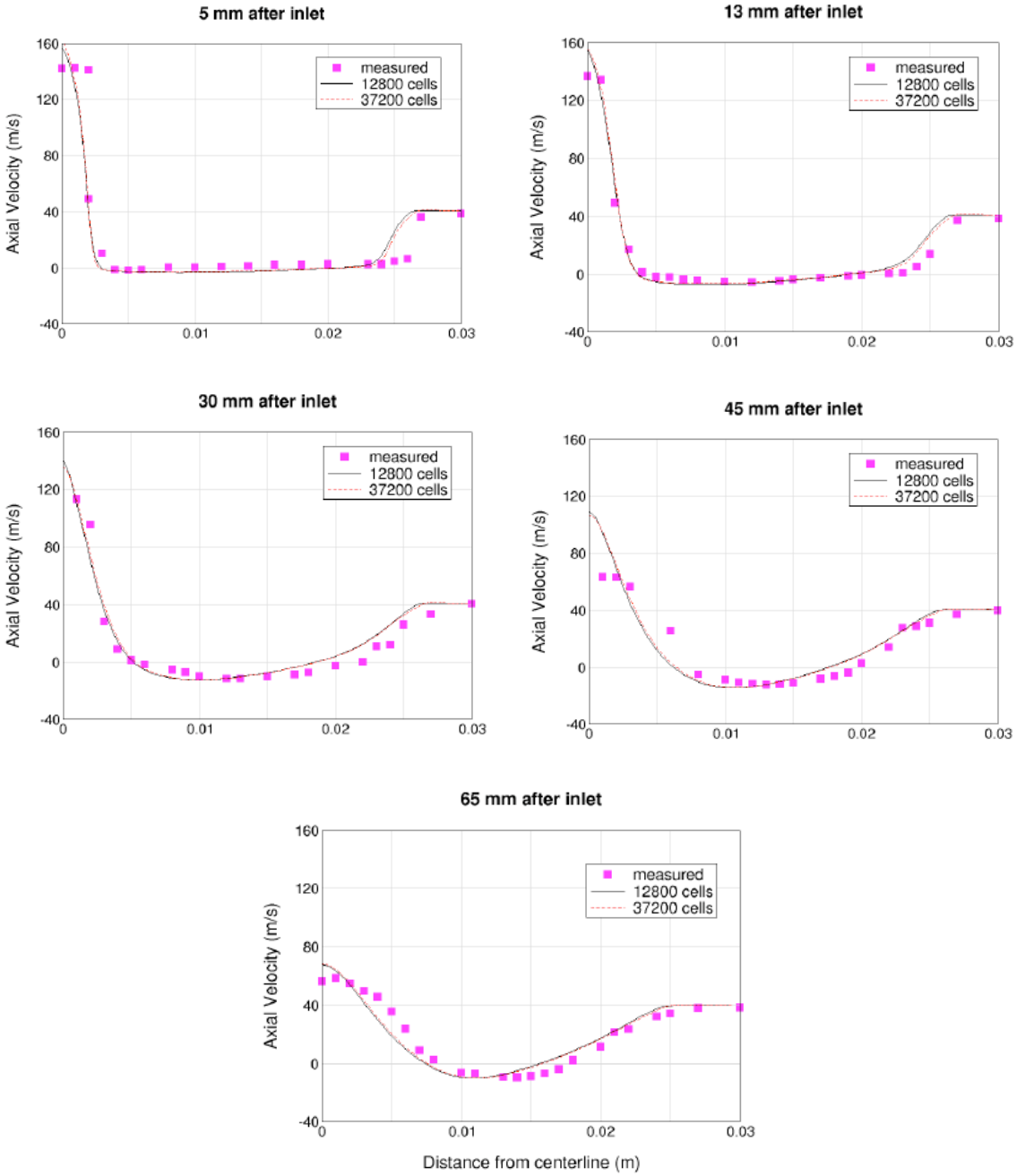

Figure 4: Radial profiles of the axial velocity at different axial stations.

(Reynolds) mean and Favre (density-weighted) mean. Because the model treats a compressible fluid and gives Favre-averaged results, we thus use that type of measurements in the comparison. However, for the velocity components, only the Reynolds average is reported in the experimental work. This strictly speaking introduces an error in the comparison. However, when we examined the difference between the Favre and Reynolds averages in some scalar quantities, we found the differences to be generally small, thereby ameliorating the impact of this inconsistency in the comparison. Our model is unsteady, but we wait for a sufficient time until a steady state is reached so that we can perform sampling of the desired fields and export the data to external data files. This was necessary because the solver we used does not allow an unsteady solution.

We start with the radial profiles of the axial velocity component at successive axial stations after the jet inlet, which are presented in Figure **4**. As expected, the variation in the axial velocity is sharp near the burner but they decay downstream due to diffusion. At the first axial station, located 5mm after the bluff-body face, we can recognize the value of the coflow entrance velocity, being 40m/s. For the fuel-jet, although the mentioned velocity in Table **1** is 118m/s, we see a higher value near 160m/s at the centerline. This is because the tabulated value is a bulk (average) value, but the actual centerline should exceed it. Despite that this station is perhaps the most-critical station in the domain, the model predictions show an overall agreement with the measurements, capturing the steep velocity drop at the edge of the jet core. At all other subsequent stations, the negative axial velocity (reversed motion) represents the recirculation zone that occurs behind the bluff-body face, and it can be inferred that the recirculation zone for this flame extends for a distance moderately larger than the bluff-body diameter. The model performed very well in capturing the axial decay of the velocity. The predictions of the two mesh levels are almost identical, which indicates a mesh-independent solution and also indicates that level-1 mesh (only 12800 cells) is sufficient to study this type of problems.

Moving to the radial profiles of the radial velocity component, we present their profiles at two successive axial stations after the jet inlet in Figure **5**. Again, the variations decay away from the bluff-body face. In the immediate vicinity of the centerline, the radial velocity is positive (outward motion) but it is reversed in the neighbor area (inward motion). This is a characteristic of the entrainment caused by the jet. At 5mm after the burner end, the overall pattern is predicted correctly by the model, but the solution with level-1 mesh shows small oscillations at the edge of the bluff body, being the interface between the recirculation zone and the coflow. However, these oscillations are eliminated when the mesh is refined as seen in level-2 solution. Despite this, the intensity of these wiggles is very small; also level-1 solution is nearly identical to level-2 solution elsewhere. Thus, level-1 mesh may still be satisfactorily employed, taking advantage of the resulting gain in simulation speed. At 13mm after the burner, the measured profile of the radial velocity exhibits discernible irregularity unlike the smooth profile in the upstream station. The model predictions are smoother but they capture well the overall profile shape. The wiggles for level-1 solution are much weaker now, and are again diminished in level-2 solution.

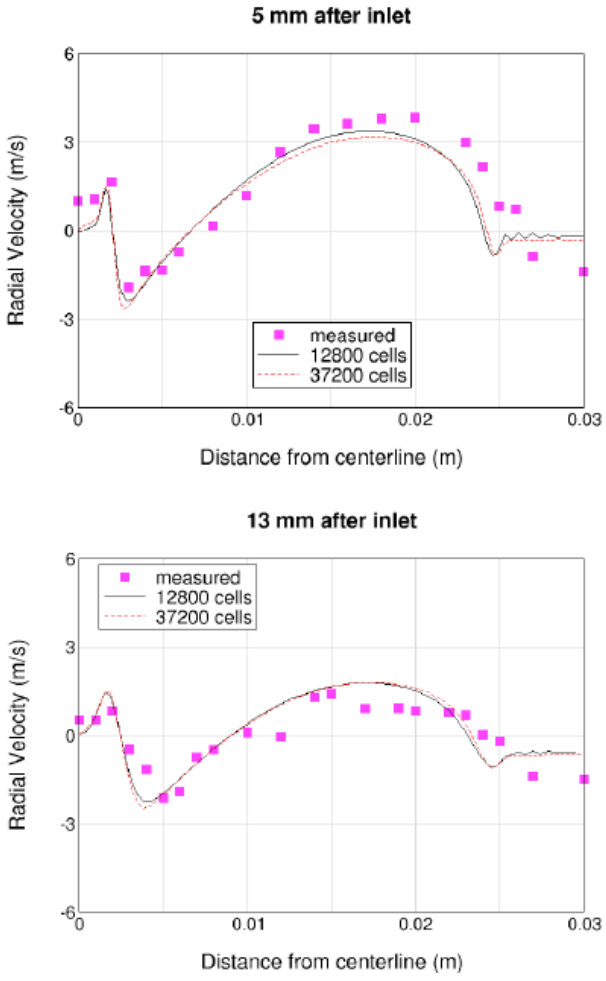

Figure 5: Radial profiles of the radial velocity at two axial stations.

At 13mm after the burner face (that is about 50% bluff-body radius downstream); the mass fractions of

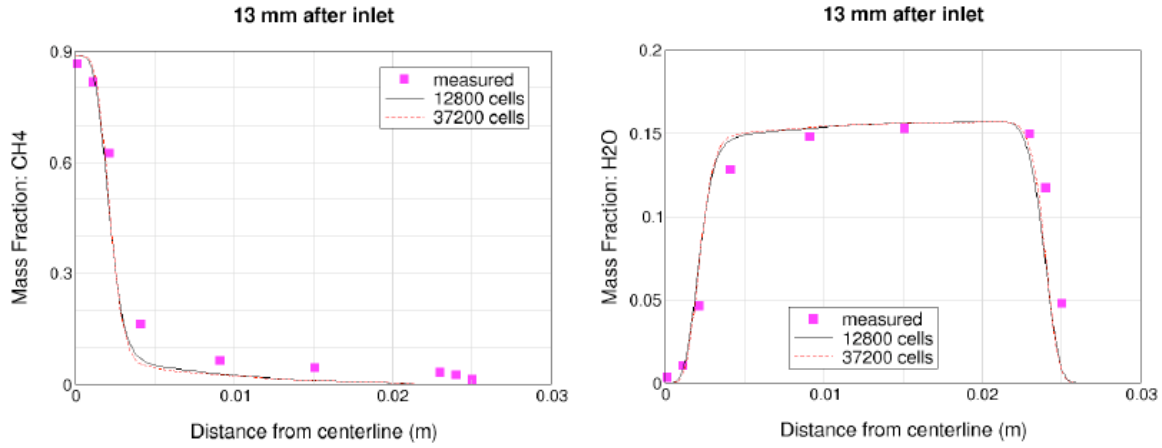

Figure 6: Radial profiles of the CH_4 and H_2O mass fractions at 13mm downstream.

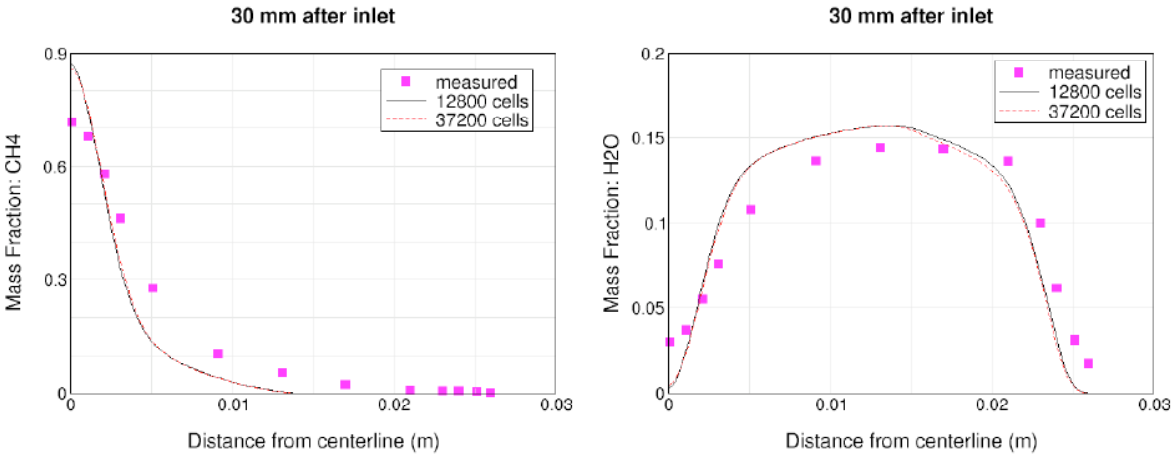

Figure 7: Radial profiles of the CH_4 and H_2O mass fractions at 30mm downstream.

one reactant (CH_4) and one product (H_2O) are presented in Figure **6**. Given the 50%/50% volume (molar) composition of CH_4 and H_2 in the fuel, the corresponding mass fractions are 0.889 for CH_4 and 0.111 for H_2. The center of the fuel-jet core still maintains the inlet mass fraction as seen in the figure for CH_4, but it drops steeply and monotonically due to the combined effect of diffusion and chemical reaction. The hat-shaped profile of the H_2O mass fraction manifests the role of the recirculation zone behind the bluff-body face, where hot combustion products are present to sustain the flame. The model predicts the profile well for either mesh level.

The mass fractions of the same species (CH_4 and H_2O) at a farther downstream location of 30mm (that is 120% of bluff-body radius) are presented in Figure **7**. For both species, the profiles became less steep compared to their counterparts in Figure **6** as a normal consequence of diffusion. The model predictions are quite reasonable but to a less extent than the former upstream station. For CH_4, the model predicts a steeper profile with less spreading than the measured profile. A similar note is made for H_2O. The predictions are practically mesh-independent.

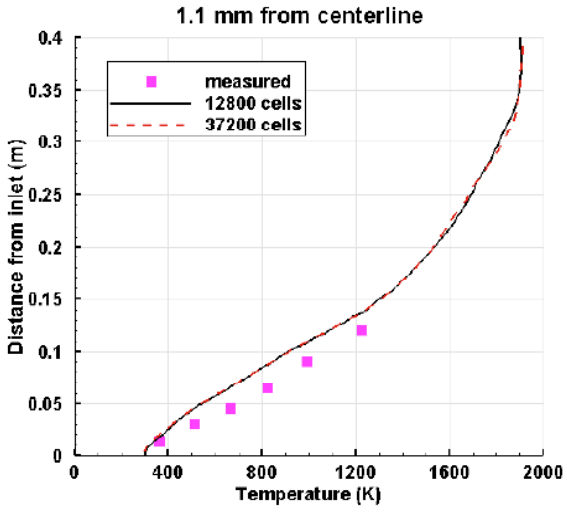

Figure 8: Axial profiles of the temperature at 1.1mm from the centerline.

We now move to the axial profiles, presenting the temperature, CH_4 mass fraction, and H_2O mass fraction at 1.1mm from the centerline (which lies within the projection of the fuel-jet orifice) in Figures **8**, **9**, and **10**, respectively. For all figures, the model results have converged in terms of the mesh resolution as seen by the almost identical predictions for both mesh levels. The temperature increases from 298 to about 1910 K at the outlet boundary. We note an underprediction of the model except in the vicinity of the burner and potentially at rear domain region (there are no sufficient measurements to decide this with confidence). The model prediction matches the measurements much better for the CH_4 mass fraction. Methane is consumed initially with a nearly constant rate, but this decelerates rapidly farther downstream as a normal consequence of the diminished concentration of reactants. In a similar but opposite manner, H_2O mass fraction increases following a nearly linear profile before it reaches a value around 0.15. The model predictions are in good agreement with the measurements.

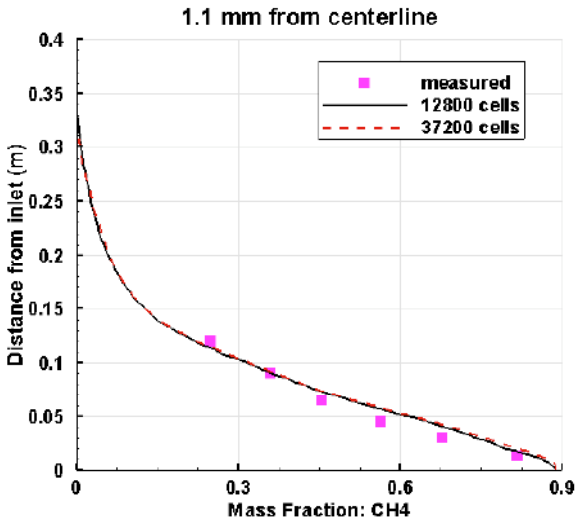

Figure 9: Axial profiles of the CH_4 mass fraction at 1.1mm from the centerline.

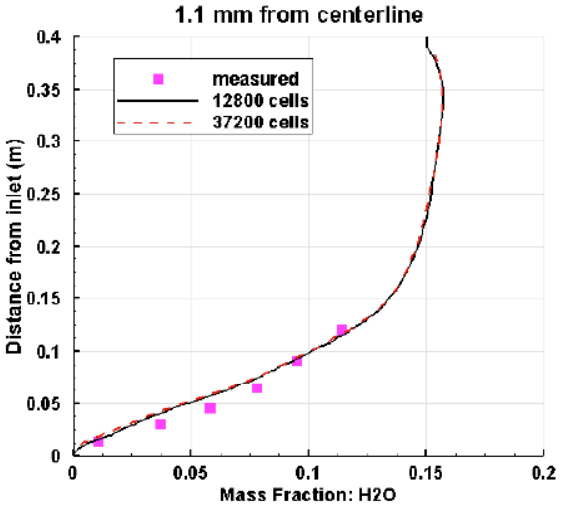

Figure 10: Axial profiles of the H_2O mass fraction at 1.1mm from the centerline.

5. CONCLUSION

Using the OpenFOAM framework, we built a computational model for turbulent nonpremixed (diffusion) flames and validated it utilizing the HM1 bluff-body high-velocity hydrogen-methane benchmark flame. The Favre-averaged Navier-Stokes equations were integrated in time and space to yield the scalar and vector fields predictions, which were then compared with reported measurements. Two multi-block structured meshes composed of 3-dimensional wedge-type cells were employed, with two levels of resolutions. The comparisons testified to the capability of the model through good agreement with measurements at different spatial locations in the domain. The effect of the grid resolution was not significant, and these flames can be satisfactorily studied by a mesh having about 10000 cells only. The model now can be used for burner design and flame analysis, forming a very useful tool for engineers in the industry. It also can be augmented further by taking advantage of other available extensions in the OpenFOAM toolkit to handle more sophisticated phenomena, such as thermal radiation (in case of very high temperatures), pulverized coal combustion, and NOx emissions.

6. ACKNOWLEDGEMENT

The author deeply appreciates valuable support from E. David Huckaby and the National Energy Technology Laboratory (U.S. Department of Energy), without which this work would not be conducted.

7. DISCLAIMER

Neither the University of Buraimi (UoB) nor any of its employees makes any warranty, expressed or implied, or assumes any legal liability or responsibility for the accuracy, completeness, or usefulness of any information, apparatus, product, or process disclosed, or represents that its use would not infringe privately owned rights. Reference herein to any specific commercial product, process, or service by trade name, trademark, manufacturer, or otherwise, does not necessarily constitute or imply its endorsement, recommendation, or favoring by the UoB. The views and opinions of the author expressed herein do not necessarily state or reflect those of the UoB.

REFERENCES

[1] Karim GA. Fuels, Energy, and the Environment, CRC Press (Taylor and Francis Group) 2012.

[2] Annamalai K and Puri IK. Combustion Science and Engineering, USA: CRC Press (Taylor and Francis Group), 2006.

[3] Zhang J and Delichatsios M. Numerical Soot Modelling and Radiation in Fires. in Proceedings of the Sixth International Seminar on Fire and Explosion Hazards, Research Publishing Service 2011.

[4] Newby JN. 21 Years of Real-World Low NOx Injection ("LNI"), in American Flame Research Committee (AFRC) Industrial Combustion Symposium, Kauai, Hawaii, USA, 2013.

[5] Londerville SB, Colannino J and Baukal JCE. Combustion Fundamentals, in The Coen and Hamworthy Combustion Handbook: Fundamentals for Power, Marine and Industrial Applications, CRC Press (Taylor and Francis Group) 2013; 25-57.

[6] Kim W, Mungal MG and Cappelli MA. Flame stabilization using a plasma discharge in a lifted jet flame (AIAA 2005-931), in 43rd AIAA Aerospace Sciences Meeting and Exhibit, Reno, Nevada, USA 2005. http://dx.doi.org/10.2514/6.2005-931

[7] YYan H, Zhang N Jiang and Ye T. Nitrogen dilution effect on stability limits of methane and propane turbulent lifted jey diffusion flame, in Advances in Energy Equipment Science and Engineering: Proceedings of the International Conference on Energy Equipment Science and Engineering, (ICEESE 2015), CRC Press (Taylor and Francis Group), 2015; 597-600.

[8] Barlow R and Frank J. Piloted CH4/Air Flames C, D, E, and F – Release 2.1 (SandiaPilotDoc21), Sandia National Laboratories, Livermore, California, USA 2007.

[9] Honeywell International Inc. Pilot Burners, Honeywell International Inc., [Online]. Available: https://customer.honeywell.com/en-US/Pages/department.aspx?cat=HonECC%20Catalog&category=Pilot+Burners&catpath=1.2.1. [Accessed 30 1 2016].

[10] JOHN ZINK COMPANY, LLC. Process Burners - Frequently Asked Questions," JOHN ZINK COMPANY, LLC, [Online]. Available: http://www.johnzink.com/parts/process-burners/faqs. [Accessed 30 1 2016].

[11] Poinsot T and Veynante D. Theoretical and Numerical Combustion - 2nd Edition, USA: R.T. Edwards, Inc 2005.

[12] Xiao F, Fujiang Y and Zhihui G. Combustion instability of pilot flame in a pilot bluff body stabilized combustor. Chinese Journal of Aeronautics 2015; 28(6): 1606-1615. http://dx.doi.org/10.1016/j.cja.2015.08.018

[13] The NEWS. Troubleshooting the Standing Pilot Safety System. BNP Media, [Online]. Available: http://www.achrnews.com/articles/85912-troubleshooting-the-standing-pilot-safety-system. [Accessed 2016 2 1].

[14] Southern California Gas Company. Gas Boilers - Advanced Design Guideline Series. New Buildings Institute, Fair Oaks, California 1998.

[15] Driscoll JF and Temme J. Role of Swirl in Flame Stabilization (AIAA 2011-108), in 49th AIAA Aerospace Sciences Meeting including the New Horizons Forum and Aerospace Exposition, Orlando, Florida 2011.

[16] Caetano NR and van der Laan FT. Turbulent Flowfield Analysis in a Bluff-Body Burner Using PIV, World Journal of Mechanics 2013; 3: 215-223. http://dx.doi.org/10.4236/wjm.2013.34021

[17] University of Sydney - Aerospace, Mechanical and Mechatronic Engineering, "Bluff-Body Flows and Flames," [Online]. Available: http://sydney.edu.au/engineering/aeromech/thermo-fluids/bluff.htm. [Accessed 28 1 2016].

[18] International Workshop on Measurement and Computation of Turbulent Nonpremixed Flames (TNF Workshop), "Experimental Data-Bluff body," Sandia National Laboratories, [Online]. Available: http://public.ca.sandia.gov/TNF/bluffbod.html. [Accessed 31 1 2016].

[19] Yan J, Thiele F and Buffat M. A Turbulence Model Sensitivity Study for CH4/H2 Bluff-Body Stabilized Flames. Flow, Turbulence and Combustion 2004; 73: 1-24. http://dx.doi.org/10.1023/B:APPL.0000044318.99203.bd

[20] Peters N. Turbulent Combustion, Cambridge: Cambridge University Press 2000. http://dx.doi.org/10.1017/CBO9780511612701

[21] Launder BE and Spalding DB. The Numerical Computation of Turbulent Flows. Computer Methods in Applied Mechanics and Engineering 1974; 3(2): 269-289. http://dx.doi.org/10.1016/0045-7825(74)90029-2

[22] Liu K, Pope SB and Caughey DA. Calculations of bluff-body stabilized flames using a joint probability density function model with detailed chemistry. Combustion and Flame 2005; 141: 89-117. http://dx.doi.org/10.1016/j.combustflame.2004.12.018

[23] Pope SB. PDF Methods for turbulent reactive flows. Progress in Energy and Combustion Science 1985; 11: 119-192,. http://dx.doi.org/10.1016/0360-1285(85)90002-4

[24] Odedra A and Malalasekera W. Eulerian particle flamelet modeling of a bluff-body CH4/H2 flame. Combustion and Flame 2007; 151: 512-531. http://dx.doi.org/10.1016/j.combustflame.2007.06.018

[25] ANSYS-Fluent, Ansys, Inc, [Online]. Available: www.ansys.com/Products/Fluids/ANSYS-Fluent. [Accessed 31 1 2016].

[26] Raman V and Pitsch H. Large-eddy simulation of a bluff-body-stabilized non-premixed flame using a recursive filter-refinement procedure. Combustion and Flame 2005; 142: 329-347. http://dx.doi.org/10.1016/j.combustflame.2005.03.014

[27] Kempf A, Lindstedt RP and Janicka J. Large-eddy simulation of a bluff-body stabilized nonpremixed flame. Combustion and Flame 2006; 144: 170-189. http://dx.doi.org/10.1016/j.combustflame.2005.07.006

[28] James S, Zhu J, Anand MS and Sekar B. Large Eddy Simulations of Bluff-Body Stabilized Turbulent Flames and Gas Turbine Combustors, in HPCMP Users Group Conference 2007 (HPCMP-UGC 2007) 2007. http://dx.doi.org/10.1109/hpcmp-ugc.2007.45

[29] Zhiyin Y. Large-eddy simulation: Past, present and the future, Chinese Journal of Aeronautics 2015; 28(1): 11-24. http://dx.doi.org/10.1016/j.cja.2014.12.007

[30] OpenCFD Ltd, "OpenFOAM® - The Open Source Computational Fluid Dynamics (CFD) Toolbox," ESI Group, [Online]. Available: http://www.openfoam.com. [Accessed 31 1 2016].

[31] Aerospace, Mechanical and Mechatronic Engineering, "Axisymmetric Bluff Body Turbulent Flow," University of Sydney, [Online]. Available: http://sydney.edu.au/engineering/aeromech/thermofluids/bluff_files/b4f3.htm. [Accessed 31 1 2016].

[32] Liu F, Ai Y and Kong W. Effect of hydrogen and helium addition to fuel on soot formation in an axisymmetric coflow laminar methane/air diffusion flame. International Journal of Hydrogen Energy 2014; 39: 3936-3946. http://dx.doi.org/10.1016/j.ijhydene.2013.12.151

[33] Marzouk OA and Huckaby ED. A Comparative Study of Eight Finite-Rate Chemistry Kinetics for CO/H2 Combustion (available online: http://jeacfm.cse.polyu.edu.hk/download/download.php?dirname=vol4no3&act=d&f=vol4no3-1_

MarzoukOA.pdf)," Engineering Applications of Computational Fluid Mechanics 2010; 4(3): 331-356.

[34] Haworth DC. Progress in probability density function methods for turbulent reacting flows, Progress in Energy and Combustion Science 2010; 36(2): 168-259. http://dx.doi.org/10.1016/j.pecs.2009.09.003

[35] Chomiak J and Karlsson A. Flame liftoff in diesel sprays. Symposium (International) on Combustion 1996; 26(2): 2557-2564. http://dx.doi.org/10.1016/s0082-0784(96)80088-9

[36] McGuirk JJ and Rodi W. The calculation of three-dimensional turbulent free jets, in Turbulent Shear Flows 1: Selected Papers from the First International Symposium on Turbulent Shear Flows, Germany, Springer-Verlag 1979; 71-83.

[37] Hossain M, Jones JC and Malalasekera W. Modelling of a bluff-body nonpremixed flame using a coupled radiation/flamelet combustion model. Flow, Turbulence and Combustion 2001; 67: 217-234,. http://dx.doi.org/10.1023/A:1015014823282

[38] Jasak H. Error analysis and estimation for the Finite Volume method with applications to fluid flows. Imperial College, University of London, London, UK 1996.

Received on 02-02-2016 Accepted on 22-02-2016 Published on 13-07-2016

DOI: http://dx.doi.org/10.15377/2409-5826.2016.03.01.2